Nano Research
2022, 15(4): 3479–3486

ISSN 1998-0124 CN 11-5974/O4
https://doi.org/10.1007/s12274-021-3874-1

Research Article

Low-power STED nanoscopy based on temporal and spatial modulation

Luwei Wang[1,§], Yue Chen[1,§], Yong Guo[1], Weixin Xie[2], Zhigang Yang[1], Xiaoyu Weng[1], Wei Yan[1] (✉), and Junle Qu[1] (✉)

[1] *Center for Biomedical Photonics & College of Physics and Optoelectronic Engineering, Key Laboratory of Optoelectronic Devices and Systems of Ministry of Education and Guangdong Province, Shenzhen 518060, China*
[2] *College of Electronics and Information Engineering, Shenzhen University, Shenzhen 518060, China*
[§] *Luwei Wang and Yue Chen contributed equally to this work.*

Received: 4 July 2021 / **Revised:** 11 August 2021 / **Accepted:** 6 September 2021

ABSTRACT

Stimulated emission depletion (STED) nanoscopy enables the visualization of subcellular organelles in unprecedented detail. However, reducing the power dependency remains one of the greatest challenges for STED imaging in living cells. Here, we propose a new method, called modulated STED, to reduce the demand for depletion power in STED imaging by modulating the information from the temporal and spatial domains. In this approach, an excitation pulse is followed by a depletion pulse with a longer delay; therefore, the fluorescence decay curve contains both confocal and STED photons in a laser pulse period. With time-resolved detection, we can remove residual diffraction-limited signals pixel by pixel from STED photons by taking the weighted difference of the depleted photons. Finally, fluorescence emission in the periphery of an excitation spot is further inhibited through spatial modulation of fluorescent signals, which replaced the increase of the depletion power in conventional STED. We demonstrate that the modulated STED method can achieve a resolution of < 100 nm in both fixed and living cells with a depletion power that is dozens of times lower than that of conventional STED, therefore, it is very suitable for long-term super-resolution imaging of living cells. Furthermore, the idea of the method could open up a new avenue to the implementation of other experiments, such as light-sheet imaging, multicolor and three-demensional (3D) super-resolution imaging.

KEYWORDS

fluorescence microscopy, super-resolution imaging, stimulated emission depletion, fluorescence lifetime, signal modulation

1 Introduction

Super-resolution microscopy (SRM) has helped to unveil details about subcellular organelles and has provided a technical foundation for further research on cellular biology [1–4]. Based on the ideas of the fluorescence on-off effect and/or molecule localization, many SRM techniques have been proposed in recent decades, such as stimulated emission depletion (STED) microscopy [5–7], single-molecule localization microscopy (SMLM) [8–10], structured illumination microscopy (SIM) [11–13], minimal emission fluxes (MINFLUX) [14–16] and their derivatives. Currently, researchers can choose a suitable SRM technique according to their research purposes. As the first far-field SRM technique, STED, which is implemented as an add-on modality to a confocal setup, is considered comparably easy to use. Furthermore, with the advantages of fast imaging and high resolution, STED has attracted great interest among biologists and has broad application prospects [17–19].

In conventional STED, an excitation beam is overlaid with a donut-shaped depletion beam so that its point spread function (PSF) is compressed and only the central region with a sub-diffraction scale can emit fluorescence [7]. One unique characteristic of STED is the ability to tune the resolution by adjusting the power of the depletion laser, which also leads to a demand for depletion power to improve the resolution [4]. Besides, to avoid the influence of re-excited fluorescence induced by the depletion laser on the image quality, a depletion wavelength at the tail of the emission spectrum of the fluorophore is usually chosen. However, the stimulated emission cross-section rapidly decreases as the depletion wavelength increases, inducing decreasing depletion efficiency and increasing demand for depletion power to achieve sufficient depletion. For this reason, current commercial STED systems usually require a depletion laser power as high as tens or even hundreds of milliwatts (up to peak intensities of 1 GW/cm^2) to achieve lateral resolution down to 10–100 nm [20]. Unfortunately, the use of intense lasers is detrimental because it causes severe photodamage in biological samples and photobleaching of fluorophores. It not only destroys the structure and function of the sample but also impedes long-term STED imaging. Therefore, reducing the demand for depletion power in STED nanoscopy is crucial to further promote its application in biological research.

To improve the spatial resolution and suppress the background for STED imaging at a low depletion power, a variety of

Address correspondence to Wei Yan, weiyan@szu.edu.cn; Junle Qu, jlqu@szu.edu.cn

techniques have been developed in recent years. The time-gated detection approach [21–23] can improve the fluorescence on-off contrast of STED images by suppressing low spatial frequencies, especially in the continuous-wave STED modality. The background suppression approach [24–26] can remove the background intensity from incomplete depletion or re-excitation by the STED beam, inducing a higher SNR in the STED images. The photon separation approach [27–30] resolves the signal into infinite dynamic components to extract the spatial high-frequency information. However, these methods cannot radically reduce the demand for depletion power in STED imaging. The recently introduced method, called digitally enhanced stimulated emission depletion (DE-STED), can achieve a resolution of ~λ/8 for biological samples with a depletion power that is an order of magnitude lower than that in conventional STED imaging [31]. In addition, Kuang et al. proposed a method in 2013, which is called fluorescence emission difference (FED), to achieve higher spatial resolution by subtracting a negative confocal image from a confocal image [32]. In FED, the two images are illuminated by doughnut-shaped and Gaussian excitation beams derived from the same laser, respectively. As a straightforward method, FED can be implemented in a simple optical system and can easily improve the resolution of confocal microscopy by a factor of 2 at ultralow laser power. The image subtraction approach has the advantage of low laser power, which usually requires two images composed of Gaussian PSF and donut-shaped PSF, respectively. However, image acquisition in different imaging modes will cause pixel mismatch between two collected images, which can distort the image quality and limit the resolution improvement of the final image, especially in living cell imaging.

Here, we introduce a new method called modulated STED (or mSTED); this method measures depleted photons and removes residual diffraction-limited signals in STED imaging by using information from the spatial and temporal domains. In this approach, an excitation pulse is followed by a depletion pulse with a longer delay than that conventional STED. With the help of the fluorescence lifetime imaging microscopy (FLIM) technique, the spatiotemporal information of the photons on each pixel is recorded so that the fluorescence decay curve contains both confocal and STED signals. Due to the time-resolved detection, we can remove residual diffraction-limited signals pixel by pixel from STED photons by taking the weighted difference of the depleted photons, which is derived from the difference in photons collected before and after the depletion pulse. Finally, fluorescence emission in the periphery of an excitation spot is further inhibited through spatial modulation of fluorescent signals, which replaced the increase of the depletion power in conventional STED. The validity of the method is demonstrated in both fixed and living cells, featuring superior quality of the final image.

2 Operating principle of modulated STED

The modulated STED method is implemented on a STED setup based on a confocal microscope with pulsed excitation and depletion lasers (Section 1 and Fig. S1 in the Electronic Supplementary Material (ESM). The excitation laser beam spatially overlaps with the depletion beam, and the two pulse trains are precisely synchronized. However, unlike conventional STED, the pulse interval between the excitation and depletion lasers is much longer and can be adjusted by a delay unit in the excitation light path. The delayed depletion pulse does not affect the previous fluorescence signal but switches off fluorophores afterward (Fig. 1(a)). All collected photons are recorded by a time-correlated single photon counting (TCSPC) module that builds up a photon distribution over the arrival time of the photons in the laser pulse period and the scan coordinates (Fig. 1(b)). The FLIM data delivered by the TCSPC system can be considered an array of pixels, each containing a large number of time channels (such as

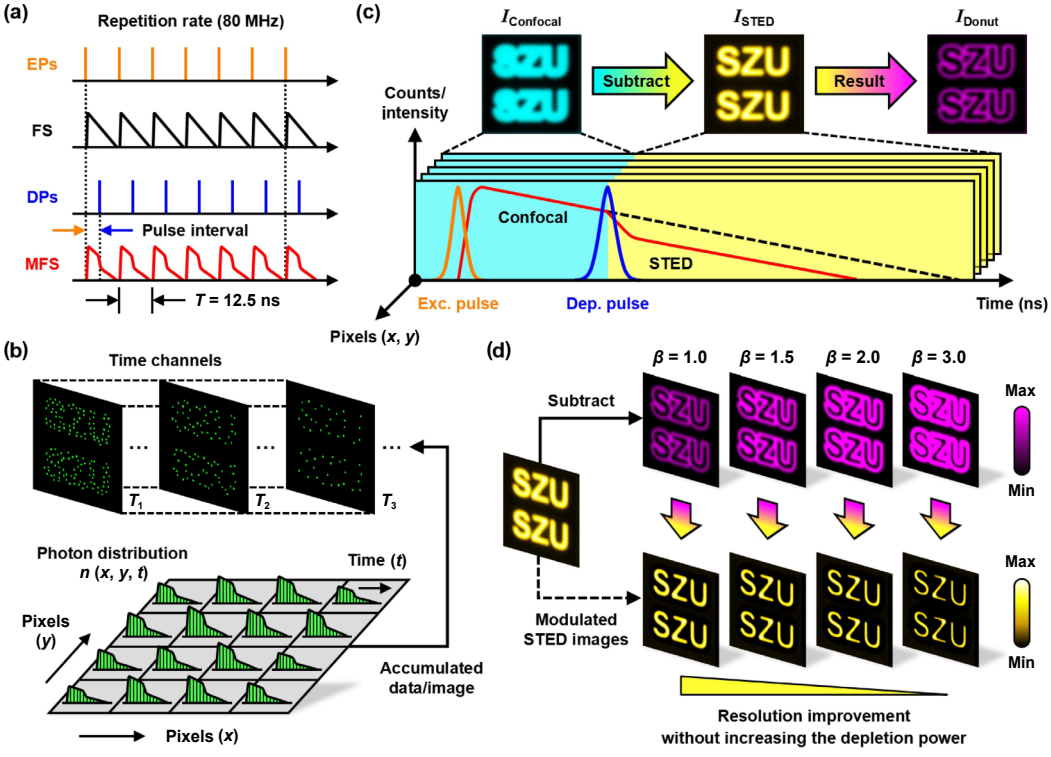

Figure 1 Scheme of modulated STED. (a) The laser pulses and the fluorescence decay curves before and after applying the depletion pluses. EPs: excitation pulses; FS: fluorescence signal; DPs: depletion pulses; MFS: modulated fluorescence signal. (b) STED fluorescence lifetime imaging based on a TCSPC module. Note that the interval between the excitation and depletion pulses is longer than that in conventional STED. (c) Temporal modulation to separate the confocal and STED photons. (d) Spatial modulation to remove the diffraction-limited signals remaining in the STED photons.

256-time channels) containing photons for subsequent times in the fluorescence decay. To obtain a lifetime image, the fit procedure has to be performed in all pixels of the image. In mSTED, however, a FLIM data file (.sdt) is divided into two parts by the depletion pulse in the time channel and binned to two separate intensity images instead of fitting the data. With this setup, the mSTED method can achieve ultralow power STED imaging with high spatial resolution and excellent image quality. This method consists of two steps: Temporal modulation to separate confocal and STED photons and spatial modulation to remove the diffraction-limited signals from STED photons.

The delayed depletion pulse divides the fluorescence signal (or fluorescence decay curve) into two parts, which is the basis of temporal modulation. For each pixel, photons emitted before and after the depletion pulse in the laser pulse period are binned to yield two separate intensity images of intensities $I_{confocal}$ and I_{STED} (Fig. 1(c)). The $I_{confocal}$ image includes the fluorescence signal from the entire region of the excitation spot, but the I_{STED} image only includes the fluorescence signal from the central region of the excitation spot. Unlike $I_{confocal}$ and I_{STED}, the intensity of the depleted photons (I_{dep}) cannot be measured directly. However, the difference between the $I_{confocal}$ and I_{STED} images can generate a donut image of the intensity I_{donut} that retains spatial information equivalent to that of the depleted photons, only with a difference in intensity. Therefore, I_{dep} can be computed by I_{donut} with a fixed ratio (α): $I_{dep} = \alpha I_{donut} = \alpha(I_{confocal} - I_{STED})$. For simplification, we use I_{donut} to represent I_{dep}, i.e., $\alpha = 1$. Based on time-resolved detection on the order of nanoseconds, the $I_{confocal}$ and I_{STED} images are considered to be acquired simultaneously, thus solving the problem of pixel mismatch in the subtraction methods based on successive image acquisition.

The I_{donut} image is critical to spatial modulation. At a fixed pulse interval, the intensity I_{donut} is increased (to I_{eDonut}) after a higher depletion power is applied. $I_{confocal}$ remains constant while I_{STED} decreases because of the enhanced depletion efficiency. The stochastic nature of stimulated emission, which can often be described by a single-exponential decay with fluorescence lifetime, implies a fixed ratio $\beta = I_{eDonut}/I_{donut}$ that is greater than 1. Therefore, the I_{eDonut} image can be obtained by multiplying the I_{donut} image by a weight coefficient (β) at a low STED power. Then, spatial modulation was performed by subtracting the enhanced I_{donut} from I_{STED}. Thus, the intensity of the final super-resolution image (the mSTED image) can be computed as a weighted difference: $I_{mSTED} = I_{STED} - I_{eDonut} = I_{STED} - \beta I_{donut}$. In this way, the depletion efficiency is enhanced without increasing the depletion power, and only the photons in the very center of the excitation spot are left in the mSTED image (Fig. 1(d)). When the intensity of pixels in the enhanced donut image is greater than that in the I_{STED} image, negative values appear in the I_{STED} image during the process of image subtraction. This indicates that the saturated stimulated emission has been reached, as in the case of high-power STED imaging. Because the I_{mSTED} image is derived from the I_{STED} image, I_{mSTED} should be between the maximum and minimum values of I_{STED}. Therefore, the negative values can be clipped to zero without the loss of super-resolution signals from the very center of the excitation laser spot [31, 33]. By collecting fluorescence decay histograms using TCSPC, we can determine I_{donut} by factors such as the pulse interval, the depletion wavelength, and the depletion power. Due to the pixel-by-pixel subtraction in real time and adjustable weighted difference, the mSTED image can be obtained at very low depletion power and features superior image quality with theoretically unlimited resolution. The detailed mathematical derivation of modulated STED imaging is presented in the ESM (subsection 2).

3 Results and discussion

3.1 Modulated STED imaging of fluorescence beads

To demonstrate the validity and broad applicability of the method, we used fluorescent beads with a diameter of 23 nanometers provided by GATTAquant. The fluorescent beads were labeled with ATTO 647N dye, which has spectral properties suitable for the optical system (Fig. 2(a)). The maximum absorption and emission wavelengths of the fluorophore were 646 and 664 nm, respectively. The depletion wavelength was tuned to 710 nm to compromise between depletion efficiency and re-excitation. The pulse interval between the excitation and depletion lasers (defined by the distance between two pulse peaks) was adjusted to 1 ns, and the pulse widths were 151 and 334 ps, respectively (Fig. 2(b)). A FLIM image was collected by applying a depletion power of 1.95 mW. Figure 2(c) shows the fluorescence decay curve (red line) after activating binning of all pixels inside the image, which was divided into two parts by the depletion pulse in the laser pulse period. The channel where the peak of the depletion pulse was located was treated as the boundary (the 60th channel). Photons in the front and back parts of the 60th channel were binned to separately yield confocal and STED images of 8 bits (the first two images in Fig. 2(d)). The last picture of Fig. 2(d) is the intensity image composed of the photons in all time channels. Because of the stimulated depletion effect, the resolution of the STED image was higher than that of the confocal image. Then, a donut image (I_{donut}) was generated by subtracting the intensity of the STED from that of the confocal. Low-pass filtering was applied to generate an evenly distributed signal from sparse photons, helping to achieve sufficient and effective depletion in modulated STED (Fig. 2(e)). The processing procedure is given by Fig. S2 in the ESM. The intensity of the I_{donut} image was greatly increased through multiplication with a weight coefficient of 16, yielding an enhanced donut image (Fig. 2(e)). Finally, the mSTED image was obtained by subtracting the enhanced donut image from the original STED image (Fig. 2(f)).

We applied two different criteria to provide quantitative resolution measurement. First, we calculated the resolution by using the mean full width at half maximum (FWHM). The FWHM was given by Gaussian fitting of the intensity profile of a single bead. The improved resolution of the mSTED was evident from calculating FWHM values from twenty beads, yielding 187.9 ± 21.0 nm for the STED image and 41.2 ± 8.0 nm for the mSTED image (Fig. 2(g)). Another resolution assessment was given by decorrelation analysis (DCA) based on an individual image without further requirements or a priori knowledge [34]. In this method, the resolution was expressed as $2/k_c$, where k_c is the cutoff frequency. A precision value of 46.94 nm (k_c = 42.61 /μm) for the mSTED image was obtained by using decorrelation analysis (Fig. 2(h)). Finally, a resolution higher than 50 nm was achieved in the mSTED image at a depletion power as low as 1.95 mW. The comparison of the STED and mSTED images revealed an impressive resolution improvement with the mSTED method.

In mSTED, the spatial resolution improves with increasing weight coefficient. We obtained a series of mSTED images with increasing coefficients at the depletion power of 1.0 and 1.95 mW (Fig. S3 in the ESM). Decorrelation analysis was used to assess the resolution. When the weight coefficient changed from 0 to 40, the resolution was increased more than fourfold at the depletion power of 1.95 mW (Fig. S4 in the ESM). By applying more than 25 mW of depletion power (measured at the front aperture of the objective lens), we achieved a resolution of approximately 40 nm in the imaging of the same fluorescent bead sample in a

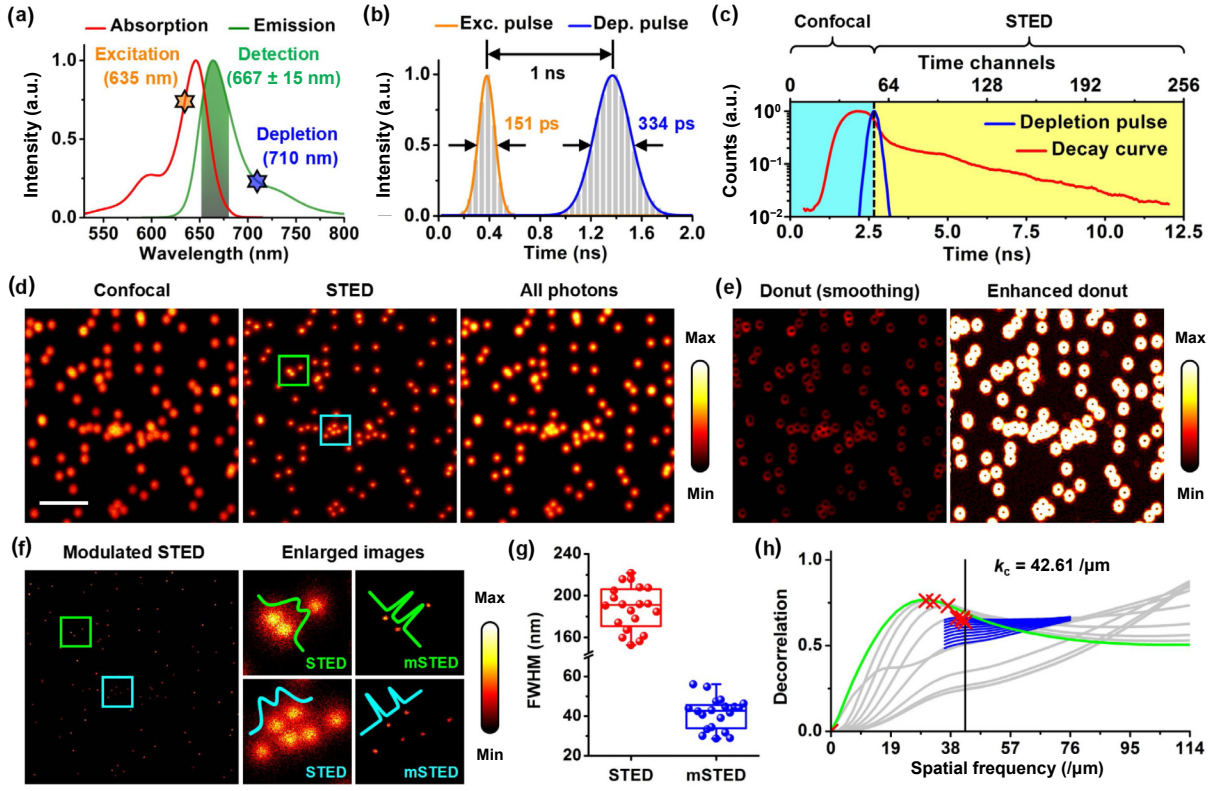

Figure 2 Modulated STED imaging of fluorescent beads. (a) Absorption and emission spectra of ATTO 647N and optical parameters of the setup. (b) The width of the excitation and depletion pulses and the pulse interval measured by TCSPC. (c) Fluorescence decay curve of a FLIM image at a depletion wavelength of 710 nm and depletion power of 1.95 mW. (d) Intensity images composed of the photons from the confocal, STED, and all time channels. Scale bar: 2 μm. (e) The donut image smoothed by low-pass filtering and an enhanced donut image with a weight coefficient of 16. (f) The modulated STED image and enlarged images from the green and cyan squares in the STED image of (d) and the modulated STED image of (f). (g) Resolution measurement from the mean FWHM of twenty beads. (h) Resolution estimation from decorrelation analysis.

commercial STED microscope (Leica SP8 STED 3X, TCS SP8 STED 3X, Leica Microsystems, Wetzlar, Germany) (Fig. S3 in the ESM. [31]). Therefore, we achieved the same resolution in modulated STED with less than a tenth of the depletion power used in conventional STED. It is widely known that the increase in the image resolution is accompanied by a decrease in the mean intensity. mSTED is no exception, but its peak intensity remains high even at very high coefficients (Fig. S5(a) in the ESM). We used the SNR and peak SNR (PSNR) as the specifications to assess the image quality. To minimize the impact of excessive mean squared error (MSE) between the original image and the target image, we used an mSTED image whose weight coefficient was 1 less than that of the target image as the original image. The results show that our method realized increasing SNR and PSNR as the weight coefficient increased, which indicated the excellent quality of the mSTED image (Section 3 and Fig. S5(b) in the ESM).

In conventional STED, the spatial resolution can be improved only by increasing the depletion power. However, for mSTED, the optimal resolution that can be realized is closely related to the specifics of the donut PSF, which is a major difference from conventional STED. In the mSTED method, the donut PSF can be classified into three types according to the intensity distribution at the center, which is determined by the relative peak intensity of the confocal and STED PSFs. A detailed analysis of the mSTED approach in three situations by computational modeling is presented in the ESM (Section 4 and Fig. S6 in the ESM). Similar to but not identical to STED, mSTED can achieve unlimited resolution in theory based on the critical donut PSF. Most importantly, the critical donut PSF in mSTED can be generated by adjusting the optical parameters, such as the pulse interval, the depletion wavelength, and the depletion power, which lays the foundation for low-power super-resolution imaging. We performed more experiments to study the effects of these parameters on mSTED imaging, as presented in the ESM (Section 5, and Figs. S7 and S8 in the ESM). Significantly, the re-excitation effect appears and becomes severe at a higher power when the depletion wavelength is shifted to 690 nm (Fig. S8 in the ESM). The re-excitation photons make the resolution of the STED image worse because the size of the donut-shaped depletion beam is larger than that of the Gaussian excitation beam in the focal plane. Therefore, the intensity difference between the confocal and STED images is not representative of the donut image composed of depleted photons, which indicates that re-excitation photons are detrimental to the method and should be avoided. In short, mSTED allows super-resolution images to be taken at an ultralow depletion power by adjusting the pulse interval and/or the depletion wavelength, which is beneficial when imaging fixed or living biological samples stained with weakly photostable fluorophores.

3.2 Modulated STED imaging of fixed and living biological cells

The ability of mSTED to improve the resolution at a low depletion power is also effective when imaging subcellular structures. To demonstrate this advantage, microtubules of esophageal carcinoma cells (KYSE-150 cells) immunolabeled with primary (anti-tubulin antibody, ab6160, Abcam) and secondary (goat anti-rat IgG STAR 635, Abberior) antibodies were used as the sample. Experiments were performed with different optical parameters. At a pulse interval of 1.2 ns and a depletion wavelength of 730 nm, a resolution of ~λ/6 was achieved in mSTED images of fixed KYSE-150 cells with the application of a depletion power of 2.34 mW and two weight coefficients (Fig. S9 in the ESM). The images were

deconvoluted with the Huygens software to improve the image quality (Section 6). In this case, an increase in the weight coefficient did not improve the resolution but reduced the image intensity and SNR of the mSTED because the confocal PSF had a higher peak intensity than the STED PSF, meaning that the donut PSF had a nonzero intensity in the center. Figure S10 in the ESM shows that mSTED imaging of fixed KYSE-150 cells (raw data) with increasing weight coefficient at two pulse intervals. The results show that the value of β is closely related to the pulse interval, and a smaller pulse interval allows for lower power and higher resolution in mSTED.

Based on a series of experiments, the depletion wavelength and the pulse interval were ultimately determined to be 730 nm and 700 ps, respectively. First, a fluorescence lifetime image was collected by applying a depletion power of 3.2 mW. Then, temporal modulation of the FLIM data was performed to acquire synchronized confocal and STED images (Figs. 3(a) and 3(b)). The comparison of the images in Fig. 3(b) shows that the resolution of the STED image was not significantly improved due to the extremely low depletion efficiency at the extended pulse interval and a low depletion power. The donut image formed by the intensity difference between the confocal and STED images (raw data) is presented after smoothing processing and adjusting the image contrast, showing the hollow intensity distribution along the labeled structures (Fig. 3(c)).

For comparison, we obtained mSTED images with weight coefficients of 2, 6, and 12; these images featured gradually improved resolution (Fig. 3(d)). Closer inspection of the enlarged images shows that the background signal around the microtubules in the regular STED image was efficiently removed by spatial modulation. The effect is also clearly visible in the intensity profiles plotted in Fig. 3(e). The profiles were Gaussian fitted, and the FWHM value decreased from 186.4 nm for the STED image to 65.2 nm for the mSTED image with a weight coefficient of 12. More precisely, the improved resolution of the mSTED images was evident from the average FWHM values over 32 representative cross-sections of microtubules, which were 184.3 ± 18.3 nm for the regular STED image and 121.4 ± 15.1 nm, 97.1 ± 13.6 nm, and 67.3 ± 10.1 nm for the mSTED images (Fig. 3(f)).

Dense fibrillar components (DFCs) are one of the essential morphologically distinct subregions of mammalian cell nucleoli for rDNA transcription and pre-rRNA processing [35, 36]. Therefore, fibrillarin in HeLa cells was immunolabeled with primary (anti-fibrillarin antibody, ab5821, Abcam) and secondary (goat anti-rabbit IgG STAR RED, Abberior) antibodies and imaged in modulated STED imaging mode (Fig. S11 in the ESM). Compared with that of the confocal image, the resolution of the STED image was improved from 305.8 ± 41.2 nm to 196.5 ± 35.6 nm (pulse interval: 700 ps; depletion wavelength: 730 nm; depletion power: 3.2 mW). In particular, a stem-loop structure of fibrillarin is shown in the mSTED image with a resolution of 92.1 ± 11.8 nm, which is consistent with the results of the study in Ref. [35]. The mSTED method can also improve the signal-to-background ratio (SBR) of low-power STED images of three-dimensional (3D) structures (Fig. S11(d) in the ESM). The SBRs, calculated as the ratio between the average intensities from the fibrillarin centers and regions between fibrillarin, were 1.9 ± 0.7 for STED and 17.5 ± 7.0 for mSTED, showing a ninefold improvement in background suppression for mSTED (Fig. S11(e) in the ESM).

To further examine the performance of the mSTED method in living cells, we studied the dynamic and subtle morphological changes within microtubules by time-lapse imaging. Microtubules

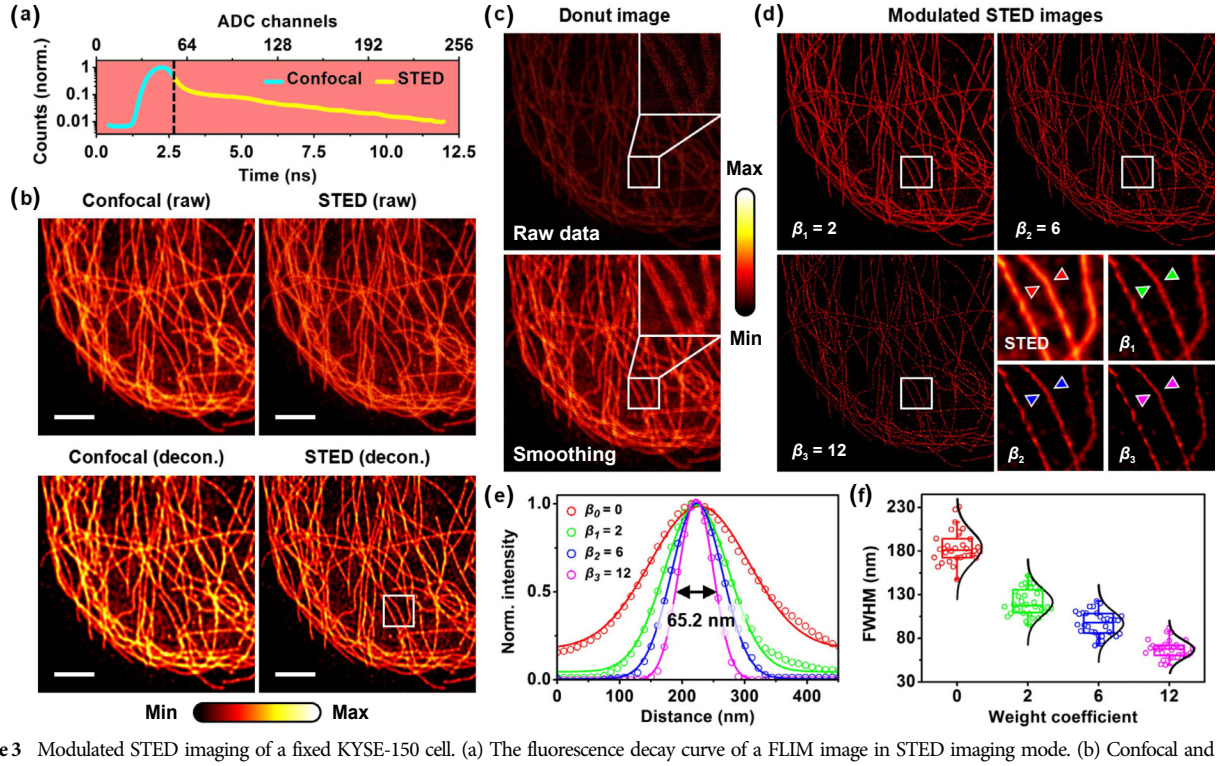

Figure 3 Modulated STED imaging of a fixed KYSE-150 cell. (a) The fluorescence decay curve of a FLIM image in STED imaging mode. (b) Confocal and STED images obtained by temporally modulating the FLIM data. Scale bar: 4 μm. (c) The donut image smoothed by low-pass filtering. (d) Modulated STED images with weight coefficients of 2, 6, and 12 and images enlarged from the white squares in (b) and (d). (e) Normalized cross-section intensity profiles (empty circles) along the arrows in the enlarged images of (d). The solid lines are Gaussian fitting curves that yield FWHM values of 186.4, 121.6, 96, and 65.2 nm for the mSTED images with weight coefficients of 0, 2, 6, and 12, respectively. (f) FWHM values of the intensity profiles of the microtubules imaged using the modulated STED method, plotted as a function of the weight coefficient. The powers of the 635 nm laser used for excitation and the 730 nm laser used for depletion at the front focal plane of the objective were 14 μW and 3.2 mW, respectively. Pulse interval: 700 ps; pixel size: 10.7 nm; field of view: 21.6 μm × 21.6 μm.

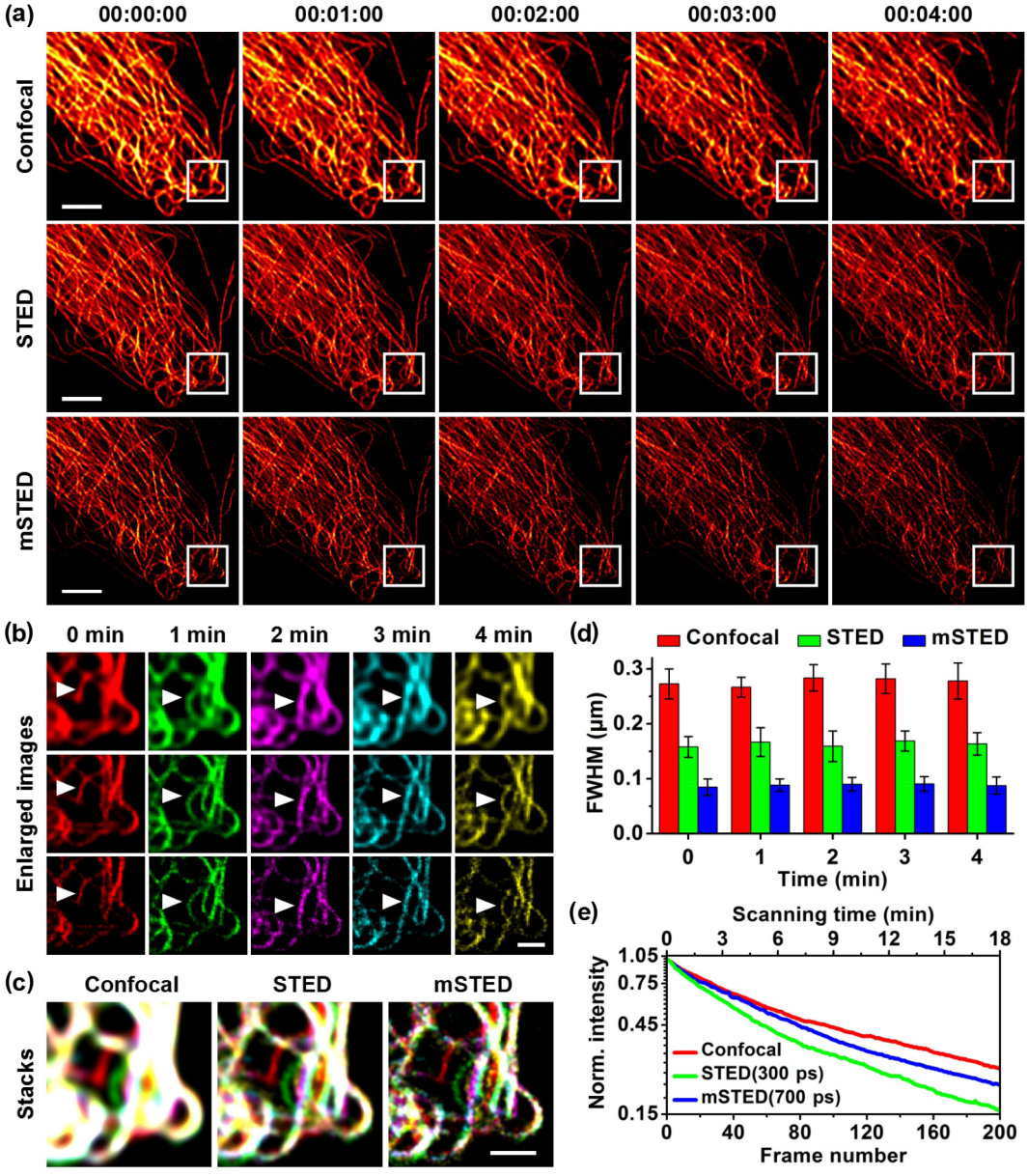

Figure 4 Modulated STED imaging of microtubules in living HeLa cells. (a) Time-lapse confocal, STED, and modulated STED images of the microtubules. Scale bar: 4 μm. (b) Close-ups of the region marked in a taken in three imaging modes. Scale bar: 1 μm. (c) Color-coded stack images (different colors indicate different imaging times). Scale bar: 1 μm. (d) Resolutions of confocal, STED, and mSTED images at different times. (e) The variation in the average intensity of the image over time in confocal, conventional STED, and modulated STED imaging modes (pixel dwell time: 5.15 μs; depletion wavelength: 730 nm; depletion power: 1.8 mW).

of HeLa cells were labeled with Tubulite™ Red (Cell Navigator™ Live Cell Tubulin Staining Kit, AAT Bioquest). Five FLIM images were obtained in modulated STED imaging mode with a pulse interval of 700 ps. Figure 4(a) shows the dynamics of microtubules in a living HeLa cell visualized with confocal, STED, and mSTED, respectively (acquisition time: 10 s; time-lapse: 1 min; excitation laser: 14 μW at 635 nm and STED laser: 1.8 mW at 730 nm on the sample plane). The enlarged images from the white squares in Fig. 4(a) were coded in false colors, and the time-lapse images were stacked for comparison (Figs. 4(b) and 4(c)). The cross-sections of microtubules revealed that the mSTED images featured both superior image quality and resolution, with FWHM values of 277.9 ± 32.9 nm for confocal, 163.5 ± 20.5 nm for STED, and 87.7 ± 15.7 nm for mSTED (Gaussian fitting, averages over ten representative cross-sections) (Fig. 4(d)). Although the time-lapse STED images had better resolution than the confocal images, many spatial structures remained unresolved. The mSTED images had higher resolution and revealed more details regarding the dynamic changes of the microtubules than the STED images. Importantly, the resolution of mSTED images was almost constant at ~ 90 nm within at least 4 min. Figure 4(e) shows the variation in the average intensity of the image over the scanning time in confocal, conventional STED (pulse interval: 300 ps), and modulated STED (pulse interval: 700 ps) imaging modes. Compared to confocal, the decay rate of the conventional STED intensity was increased by applying a depletion laser with a power of 1.8 mW. However, the intensity of the mSTED image decayed slowly compared to that of conventional STED at the same depletion power, indicating a reduced photobleaching rate. Therefore, the mSTED method, with a large time delay between the excitation and depletion pulses, is conducive to resisting photobleaching and extending the effective time in living cell imaging. The power density of the excitation and depletion lasers was calculated to be 9.64 kW/cm^2 for 14 μW excitation power and 420.8 kW/cm^2 for 1.8 mW depletion power (Section 7 and Fig. S12 in the ESM). The power density of the depletion laser in the focal plane was 43.7 times that of the excitation laser; however, it was dozens or even hundreds of times lower than that in conventional STED for realizing the same resolution, which is very helpful for the applications of STED nanoscopy in living cell

imaging.

4 Conclusions

mSTED achieves a resolution of ~λ/9 in fixed cells and a resolution of ~λ/7 in living cells with a depletion power that is dozens of times lower than that of conventional STED imaging. As a low-power super-resolution imaging technique that combines the physical principle of stimulated emission, time-correlated single photon detection, and mathematical processing of fluorescence signals, mSTED nanoscopy measures the temporal and spatial information of confocal and STED photons in real time and improves the depletion efficiency by increasing the intensity of the depleted photons. Consequently, the method relaxes the constraints on fluorophores with lower photobleaching resistance, e.g., fluorescent proteins with higher cell affinity, and on lasers with lower peak power to achieve the same resolution. Implementation of the mSTED method requires a rather simple modification to a pulsed STED fluorescence lifetime imaging microscope, i.e., the adjustment of the time interval between two laser pulses. The mSTED method also has time-gated detection capabilities because the confocal photons between the excitation and depletion pulses are completely removed in the final super-resolution image.

From a functional perspective, the subtraction factor γ in FED is similar to the weight coefficient β in mSTED. However, the values of γ and β in the final super-resolution image are different because of the imaging principle. In FED, the factor γ mainly depends on the power of the excitation laser. While the weight coefficient β is affected by several parameters in mSTED, such as the pulse interval, depletion wavelength, and depletion power. In summary, mSTED differs from FED in the imaging principle and the image acquisition method. As a data processing method, FED involves two physical processes of stimulated absorption and spontaneous emission, while mSTED also includes a third process of stimulated emission. Therefore, the subtracted image is composed of fluorescent photons in FED, while it consists of stimulated emission photons in mSTED. In FED, the negative confocal image is formed under the donut-shaped excitation, which has a larger size or area than the Gaussian excitation in the focal plane. When the distance between the objects is less than half the diameter of the donut-shaped beam, it will cause the loss of signal in the process of image subtraction, resulting in a reduction in the peak intensity of the final image and the limited resolution. Different from FED, the donut image in mSTED is composed of the depleted photons, which is obtained by making a subtraction between the $I_{confocal}$ and I_{STED} images. Therefore, the diameter of the donut PSF in mSTED is much smaller than that in FED, which alleviates the problem of signal loss in the data processing. As a result, the peak intensity of mSTED image can remain at a high level, inducing superior quality and higher resolution than that in FED. In addition, the confocal image and the negative confocal image in FED are captured under the illumination of a single Gaussian beam and a single donut-shaped beam, respectively. Image acquisition in different imaging modes will cause pixel mismatch between these images, which also appears in DE-STED. The pixel mismatch will reduce the quality and even resolution of the final image. Therefore, it must be seriously considered and promptly resolved. However, this problem does not arise in mSTED because the temporal resolution between the $I_{confocal}$ and I_{STED} images is in nanoseconds with the help of FLIM. The two images can be considered to be acquired simultaneously, thus perfectly solving the problem of pixel mismatch in differential imaging techniques based on successive image acquisition.

We note that there is a price for signal measurement and subtraction. Indeed, the intensity of modulated STED images is based on the photons collected after the depletion pulse and then reduced according to the depleted photons and the weight coefficient. However, we showed that the low number of signal photons does not pose a problem in practice because we can acquire highly resolved images by increasing the acquisition time to a few seconds without causing other problems, e.g., pixel mismatch or photobleaching. Although modulated STED is a powerful approach, its performance is still restricted by many factors in some cases, e.g., wavefront distortion in deep imaging and the imaging speed in observing the rapid process of a biological sample. To fully take advantage of the method, adaptive optics techniques can be utilized to reshape the beam wavefront to improve the quality of super-resolution images in imaging thick samples, and an avalanche diode (APD) detector can improve the temporal resolution by increasing the photon count rate. The idea of the method is also expected to be beneficial to other experiments, such as light-sheet imaging and multicolor imaging.

Acknowledgements

This work has been partially supported by the National Basic Research Program of China (No. 2017YFA0700500); the National Natural Science Foundation of China (Nos. 61620106016, 61835009, 62005171, and 61975127); Guangdong Natural Science Foundation (Nos. 2019A1515110380 and 2020A1515010679); Shenzhen International Cooperation Project (No. GJHZ20180928161811821); Shenzhen Basic Research Project (No. JCYJ20180305125304883); China Post-doctoral Science Foundation (No. 2019M663050).

Electronic Supplementary Material: Supplementary material (further details of the experimental setup, the mathematical derivation of modulated STED imaging, the calculation of the SNR and PSNR, three types of the donut PSFs in modulated STED, the effect of the optical parameters on modulated STED imaging, the deconvolution, the calculation of the laser power density, the sample preparation, and Figs. S1–S12) is available in the online version of this article at https://doi.org/10.1007/s12274-021-3874-1.

References

[1] Sahl, S. J.; Hell, S. W.; Jakobs, S. Fluorescence nanoscopy in cell biology. *Nat. Rev. Mol. Cell Biol.* **2017**, *18*, 685–701.

[2] Sigal, Y. M.; Zhou, R. B.; Zhuang, X. W. Visualizing and discovering cellular structures with super-resolution microscopy. *Science* **2018**, *361*, 880–887.

[3] Jin, D. Y.; Xi, P.; Wang, B. M.; Zhang, L.; Enderlein, J.; Van Oijen, A. M. Nanoparticles for super-resolution microscopy and single-molecule tracking. *Nat. Methods* **2018**, *15*, 415–423.

[4] Schermelleh, L.; Ferrand, A.; Huser, T.; Eggeling, C.; Sauer, M.; Biehlmaier, O.; Drummen, G. P. C. Super-resolution microscopy demystified. *Nat. Cell Biol.* **2019**, *21*, 72–84.

[5] Hell, S. W.; Wichmann, J. Breaking the diffraction resolution limit by stimulated emission: Stimulated-emission-depletion fluorescence microscopy. *Opt. Lett.* **1994**, *19*, 780–782.

[6] Klar, T. A.; Jakobs, S.; Dyba, M.; Egner, A.; Hell, S. W. Fluorescence microscopy with diffraction resolution barrier broken by stimulated emission. *Proc. Natl. Acad. Sci. USA* **2000**, *97*, 8206–8210.

[7] Blom, H.; Widengren, J. Stimulated emission depletion microscopy. *Chem. Rev.* **2017**, *117*, 7377–7427.

[8] Gould, T. J.; Verkhusha, V. V.; Hess, S. T. Imaging biological structures with fluorescence photoactivation localization microscopy. *Nat. Protoc.* **2009**, *4*, 291–308.

[9] Rust, M. J.; Bates, M.; Zhuang, X. W. Sub-diffraction-limit imaging

by stochastic optical reconstruction microscopy (STORM). *Nat. Methods* **2006**, *3*, 793–796.
[10] Sauer, M.; Heilemann, M. Single-molecule localization microscopy in eukaryotes. *Chem. Rev.* **2017**, *117*, 7478–7509.
[11] Gustafsson, M. G. L. Surpassing the lateral resolution limit by a factor of two using structured illumination microscopy. *J. Microsc.* **2000**, *198*, 82–87.
[12] Gustafsson, M. G. L. Nonlinear structured-illumination microscopy: Wide-field fluorescence imaging with theoretically unlimited resolution. *Proc. Natl. Acad. Sci. USA* **2005**, *102*, 13081–13086.
[13] Heintzmann, R.; Huser, T. Super-resolution structured illumination microscopy. *Chem. Rev.* **2017**, *117*, 13890–13908.
[14] Balzarotti, F.; Eilers, Y.; Gwosch, K. C.; Gynnå, A. H.; Westphal, V.; Stefani, F. D.; Elf, J.; Hell, S. W. Nanometer resolution imaging and tracking of fluorescent molecules with minimal photon fluxes. *Science* **2017**, *355*, 606–612.
[15] Eilers, Y.; Ta, H.; Gwosch, K. C.; Balzarotti, F.; Hell, S. W. MINFLUX monitors rapid molecular jumps with superior spatiotemporal resolution. *Proc. Natl. Acad. Sci. USA* **2018**, *115*, 6117–6122.
[16] Gwosch, K. C.; Pape, J. K.; Balzarotti, F.; Hoess, P.; Ellenberg, J.; Ries, J.; Hell, S. W. MINFLUX nanoscopy delivers 3D multicolor nanometer resolution in cells. *Nat. Methods* **2020**, *17*, 217–224.
[17] Willig, K. I.; Rizzoli, S. O.; Westphal, V.; Jahn, R.; Hell, S. W. STED microscopy reveals that synaptotagmin remains clustered after synaptic vesicle exocytosis. *Nature* **2006**, *440*, 935–939.
[18] Yang, X. S.; Yang, Z. G.; Wu, Z. Y.; He, Y.; Shan, C. Y.; Chai, P. Y.; Ma, C. S.; Tian, M.; Teng, J. L.; Jin, D. Y. et al. Mitochondrial dynamics quantitatively revealed by STED nanoscopy with an enhanced squaraine variant probe. *Nat. Commun.* **2020**, *11*, 3699.
[19] Spahn, C.; Grimm, J. B.; Lavis, L. D.; Lampe, M.; Heilemann, M. Whole-cell, 3D, and multicolor STED imaging with exchangeable fluorophores. *Nano Lett.* **2019**, *19*, 500–505.
[20] Vicidomini, G.; Bianchini, P.; Diaspro, A. STED super-resolved microscopy. *Nat. Methods* **2018**, *15*, 173–182.
[21] Vicidomini, G.; Moneron, G.; Han, K. Y.; Westphal, V.; Ta, H.; Reuss, M.; Engelhardt, J.; Eggeling, C.; Hell, S. W. Sharper low-power STED nanoscopy by time gating. *Nat. Methods* **2011**, *8*, 571–573.
[22] Vicidomini, G.; Schönle, A.; Ta, H.; Han, K. Y.; Moneron, G.; Eggeling, C.; Hell, S. W. STED nanoscopy with time-gated detection: Theoretical and experimental aspects. *PLoS One* **2013**, *8*, e54421.
[23] Wang, Y. F.; Kuang, C. F.; Gu, Z. T.; Xu, Y. K.; Li, S.; Hao, X.; Liu, X. Time-gated stimulated emission depletion nanoscopy. *Opt. Eng.* **2013**, *52*, 093107.
[24] Bordenave, M. D.; Balzarotti, F.; Stefani, F. D.; Hell, S. W. STED nanoscopy with wavelengths at the emission maximum. *J. Phys. D:Appl. Phys.* **2016**, *49*, 365102.
[25] Gao, P.; Prunsche, B.; Zhou, L.; Nienhaus, K.; Nienhaus, G. U. Background suppression in fluorescence nanoscopy with stimulated emission double depletion. *Nat. Photonics* **2017**, *11*, 163–169.
[26] Gao, P.; Nienhaus, G. U. Precise background subtraction in stimulated emission double depletion nanoscopy. *Opt. Lett.* **2017**, *42*, 831–834.
[27] Lanzanò, L.; Hernández, I. C.; Castello, M.; Gratton, E.; Diaspro, A.; Vicidomini, G. Encoding and decoding spatio-temporal information for super-resolution microscopy. *Nat. Commun.* **2015**, *6*, 6701.
[28] Wang, L. W.; Chen, B. L.; Yan, W.; Yang, Z. G.; Peng, X.; Lin, D. Y.; Weng, X. Y.; Ye, T.; Qu, J. L. Resolution improvement in STED super-resolution microscopy at low power using a phasor plot approach. *Nanoscale* **2018**, *10*, 16252–16260.
[29] Tortarolo, G.; Sun, Y. S.; Teng, K. W.; Ishitsuka, Y.; Lanzanó, L.; Selvin, P. R.; Barbieri, B.; Diaspro, A.; Vicidomini, G. Photon-separation to enhance the spatial resolution of pulsed STED microscopy. *Nanoscale* **2019**, *11*, 1754–1761.
[30] Chen, Y.; Wang, L. W.; Yan, W.; Peng, X.; Qu, J. L.; Song, J. Elimination of re-excitation in stimulated emission depletion nanoscopy based on photon extraction in a phasor plot. *Laser Photonics Rev.* **2020**, *14*, 1900352.
[31] Wang, L. W.; Chen, Y.; Peng, X.; Zhang, J.; Wang, J. L.; Liu, L. W.; Yang, Z. G.; Yan, W.; Qu, J. L. Ultralow power demand in fluorescence nanoscopy with digitally enhanced stimulated emission depletion. *Nanophotonics* **2020**, *9*, 831–839.
[32] Kuang, C. F.; Li, S.; Liu, W.; Hao, X.; Gu, Z. T.; Wang, Y. F.; Ge, J. H.; Li, H. F.; Liu, X. Breaking the diffraction barrier using fluorescence emission difference microscopy. *Sci. Rep.* **2013**, *3*, 1441.
[33] Vicidomini, G.; Moneron, G.; Eggeling, C.; Rittweger, E.; Hell, S. W. STED with wavelengths closer to the emission maximum. *Opt. Express* **2012**, *20*, 5225–5236.
[34] Descloux, A.; Grußmayer, K. S.; Radenovic, A. Parameter-free image resolution estimation based on decorrelation analysis. *Nat. Methods* **2019**, *16*, 918–924.
[35] Yao, R. W.; Xu, G.; Wang, Y.; Shan, L.; Luan, P. F.; Wang, Y.; Wu, M.; Yang, L. Z.; Xing, Y. H.; Yang, L. et al. Nascent pre-rRNA sorting via phase separation drives the assembly of dense fibrillar components in the human nucleolus. *Mol. Cell* **2019**, *76*, 767–783.
[36] Lafontaine, D. L. J.; Riback, J. A.; Bascetin, R.; Brangwynne, C. P. The nucleolus as a multiphase liquid condensate. *Nat. Rev. Mol. Cell Biol.* **2021**, *22*, 165–182.